2D CO CRS stack for OBS and VSP data and arbitrary top-surface topography

Tim Boelsen and Jürgen Mann

Geophysical Institute, University of Karlsruhe, Germany

Summary

In recent years, the Common-Reflection-Surface stack has been evolved as an alternative to conventional stacking methods. A new hyperbolic traveltime approximation for finite-offset to take arbitrary top-surface topography into account is presented. Based on this formula we derive a Common-Reflection-Surface stacking operator that is in principle able to handle data from vertical seismic profiles. Moreover, the application to ocean bottom seismic data is discussed. This is demonstrated with a synthetic data set yielding a stacked common-offset section with a high signal-to-noise ratio and kinematic wavefield attribute sections which can be used for further analyses.

Introduction

Several well-known stacking tools were established to simulate zero-offset (ZO) sections from multi-coverage, seismic reflection prestack data, e. g., the common-midpoint (CMP) stack and the normal-moveout(NMO)/dip-moveout(DMO)/stack sequence. However, these methods do not make full use of the available reflection energy during stacking and deliver less information for further imaging steps compared to novel approaches.

One of the novel approaches is the Common-Reflection-Surface (CRS) stack (e.g., Mann et al., 1999; Jäger et al., 2001). Compared to conventional stacking methods the CRS stack has the following advantages:

- Similarly as in high-density stacking velocity analysis, the optimum CRS stacking operator is determined fully automated by means of coherence analysis. Thus, it is an entirely *data-driven* method.
- For each sample of the section to be simulated, the operator utilizes the full multi-coverage data volume within a spatial aperture during the imaging process. The operator defines an entire *stacking surface* with a spatial extension also in midpoint direction. Thus, much more traces contribute to the CRS stack result yielding *higher signal-to-noise (S/N) ratios.*
- The parameterization of the CRS stacking operator is based on an isotropic, inhomogeneous model with curved reflectors. Therefore, the operator fits the actual reflection events in the prestack data often better than conventional methods based on simpler assumptions.
- As a by-product of the CRS stack, *kinematic wavefield attribute and coherence sections* are obtained which can be used for further applications like different kinds of inversion schemes (see, e. g., Duveneck, 2004; Müller, 2005).

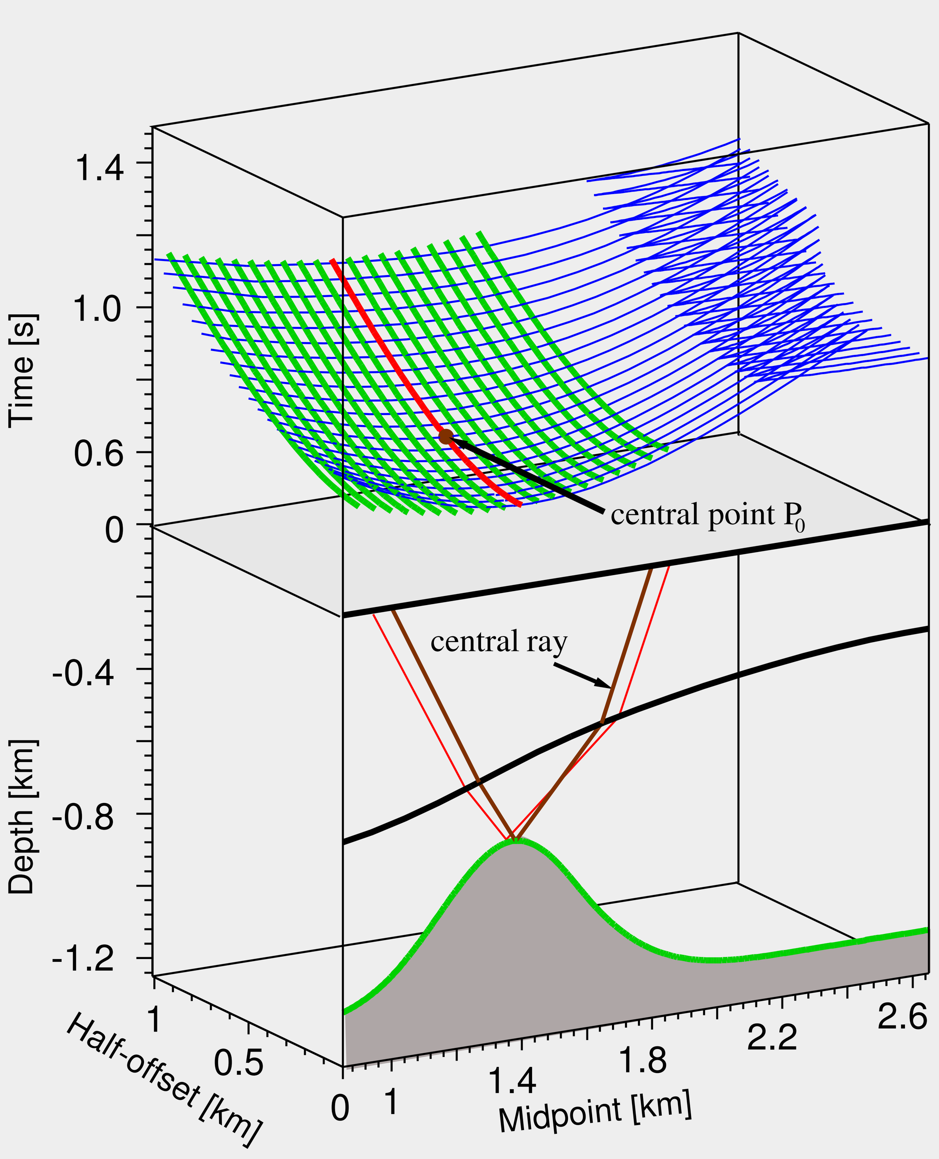

Figure 1: Lower part: a simple 2D model with homogeneous layers. Upper part: forward-calculated traveltimes of waves reflected at the second interface (blue CO traveltime curves). A central point P_0 (brown) is depicted in the (m,h,t) space associated with a central ray. The CO CRS stacking surface associated with P_0 is visualized by means of green CMP traveltime curves. Usually, only one CMP curve (red) enters into stacking velocity analysis. One paraxial ray for this selected midpoint is depicted in red.

Originally developed to simulate ZO sections, the CRS method was extended to stack prestack data into a selected finite-offset (FO) gather (Zhang et al., 2001), e. g., into a common-offset (CO) gather. Bergler (2001) showed that this so-called 2D CO CRS stacking operator can also be used to describe traveltimes of S-waves as well as PS converted waves which is of particular interest for land seismics, ocean bottom seismics (OBS), and vertical seismic profiling (VSP).

Arbitrary topography

The most general second-order paraxial traveltime approximation (e. g., Zhang, 2003) applicable in the framework of the CRS stack accounts for

- 3D data acquisition and processing,
- arbitrary top-surface topography as source and receiver elevations are explicitely considered,
- velocity gradients in the vicinity of the sources and receivers.

The traveltime formula for the 2D CO CRS stack for arbitrary topography can directly be derived from the general moveout formula given in Zhang (2003). Assuming 2D data acquisition, 2.5D subsurface models, and negligible near-surface velocity gradients, the searched-for hyperbolic traveltime formula reads

$$\begin{aligned} t^2(\Delta x_S, \Delta x_G, \Delta z_S, \Delta z_G) = \\ \left(t_0 + \frac{\sin\beta_G}{v_G}\Delta x_G - \frac{\sin\beta_S}{v_S}\Delta x_S + \frac{\cos\beta_G}{v_G}\Delta z_G - \frac{\cos\beta_S}{v_S}\Delta z_S\right)^2 \\ + t_0 D B^{-1}\left(\Delta x_G - \Delta z_G \tan\beta_G\right)^2 \\ + t_0 A B^{-1}\left(\Delta x_S - \Delta z_S \tan\beta_S\right)^2 \\ - 2 t_0 B^{-1}\left(\Delta x_G - \Delta z_G \tan\beta_G\right)\left(\Delta x_S - \Delta z_S \tan\beta_S\right). \end{aligned} \quad (1)$$

- t_0 denotes the traveltime along the central ray,
- v_S and v_G are the near-surface velocities at the source and receiver,
- Δx_S and Δx_G denote the horizontal displacements between sources and receivers of central and paraxial ray, Δz_S and Δz_G are the corresponding vertical displacements,
- β_S and β_G are the incidence and emergence angles of the central ray at source and receiver,
- A, B, and D are three elements of the surface-to-surface ray propagator matrix in a global coordinate system.

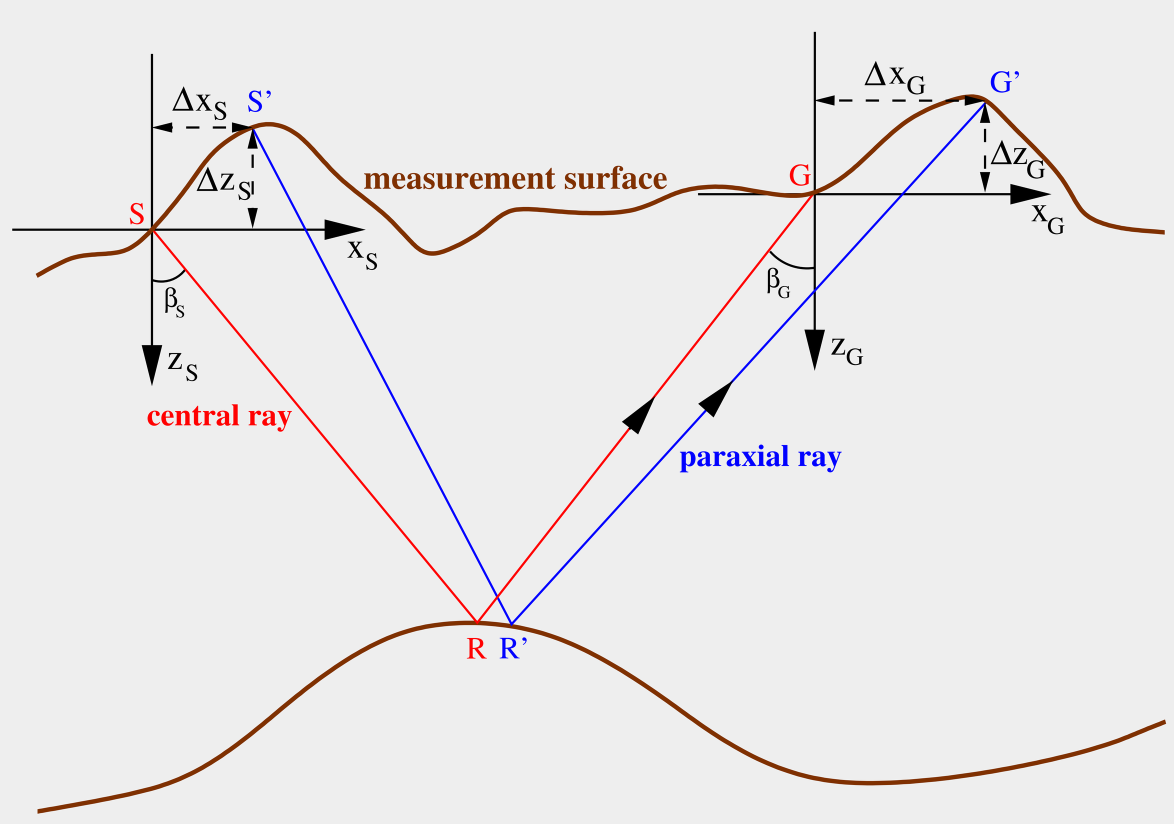

Figure 2: Measurement surface with arbitrary topography. An arbitrary central ray SRG with the incidence and emergence angles β_S and β_G is depicted in red. Also shown is an arbitrarily chosen paraxial ray $S'R'G'$ (blue) in its close vicinity.

Bergler (2001) and Zhang et al. (2001) related the elements A, B, C, and D of the ray propagator matrix to three wavefront curvatures K_1, K_2, and K_3, where K_1 is defined as the wavefront curvature of an emerging wave at the receiver in a common-shot (CS) experiment, while K_2 and K_3 are the wavefront curvatures at the source and receiver, respectively, in a (hypothetical) CMP experiment.

Ocean bottom seismics

Figure 3 shows a simple sketch of a typical 2D OBS acquisition geometry with the receivers located on the seafloor and the sources some meters below the water surface. We assume a virtually horizontal ocean bottom without significant topography and a constant source depth.

This implies $\Delta z_S = \Delta z_G \equiv 0$, see also Figure 3. Thus, Equation (1) reduces in the OBS case with the above made assumptions to

$$\begin{aligned} t^2(\Delta x_S, \Delta x_G) = \left(t_0 + \frac{\sin\beta_G}{v_G}\Delta x_G - \frac{\sin\beta_S}{v_S}\Delta x_S\right)^2 \\ + t_0\left(D B^{-1}\Delta x_G^2 + A B^{-1}\Delta x_S^2 - 2B^{-1}\Delta x_G \Delta x_S\right), \end{aligned} \quad (2)$$

Note that Equation (2) coincides with the original 2D CO CRS stacking operator (Bergler, 2001; Zhang et al., 2001) developed to stack data acquired along one straight line on a horizontal measurement surface (e. g., land seismic data or conventional marine data).

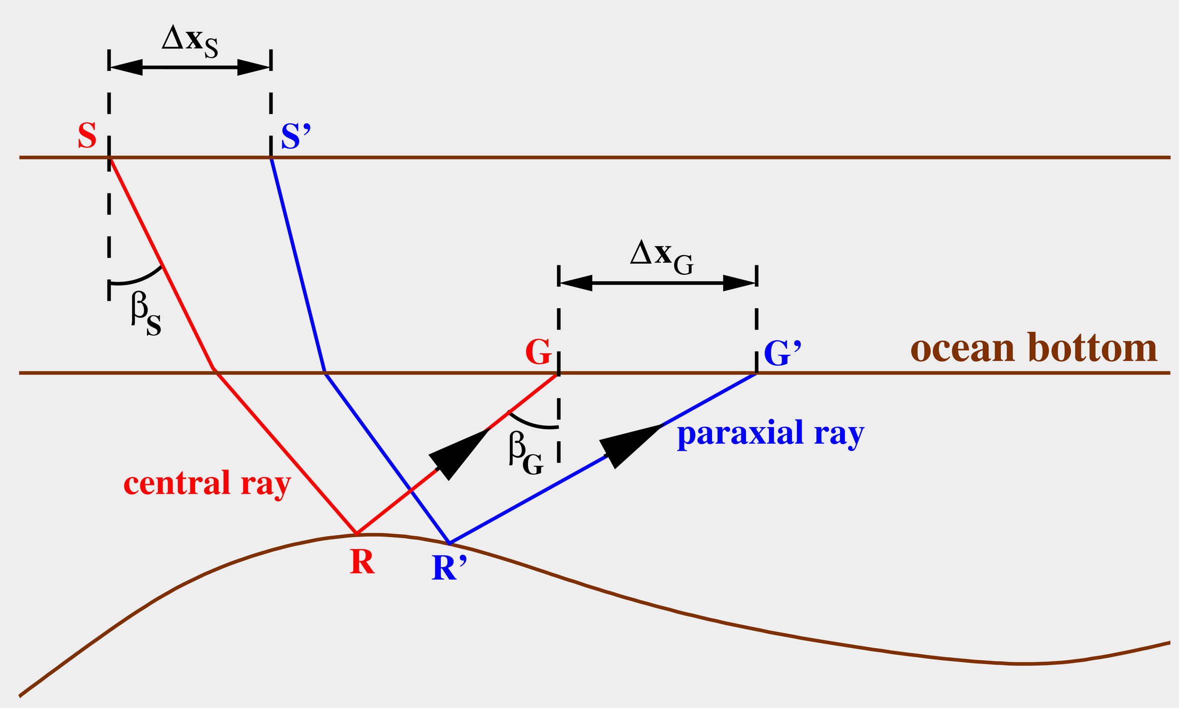

Figure 3: 2D OBS acquisition geometry. An arbitrarily chosen central ray (SRG) and a paraxial ray ($S'R'G'$) in its close vicinity are depicted in red and blue, respectively.

If there is significant topography present at the ocean bottom, it is possible to use Equation (1) to take the topography into account. This does not affect the simplifying assumption $\Delta z_S \equiv 0$.

Vertical seismic profiling

A typical 2D VSP acquisition geometry is characterized by receivers placed in a borehole while the sources are located along a straight line on the top-surface, see also Figure 4. We assume a vertical borehole and that all sources are disposed at the same level, i. e., on a measurement surface on land without topography or in the same water depth in marine environments. Thus, the vertical displacements between the sources Δz_S and the horizontal displacements between the receivers Δx_G vanish, i. e., $\Delta z_S = \Delta x_G \equiv 0$. With these assumptions, Equation (1) simplifies to

$$\begin{aligned} t^2(\Delta x_S, \Delta z_G) = \left(t_0 - \frac{\sin\beta_S}{v_S}\Delta x_S + \frac{\cos\beta_G}{v_G}\Delta z_G\right)^2 \\ + t_0\left(D B^{-1}\tan\beta_G^2 \Delta z_G^2\right. \\ \left. + A B^{-1}\Delta x_S^2 + 2B^{-1}\tan\beta_G \Delta z_G \Delta x_S\right). \end{aligned} \quad (3)$$

Furthermore, CRS stacking operators for so-called reverse VSP and cross-well acquisition geometries can easily be derived by means of Equation (1), see Boelsen (2005). In the former case, the sources are placed downhole while the receivers are deployed at the surface. Thus, $\Delta x_S = \Delta z_G \equiv 0$, assuming a vertical borehole and a horizontal measurement surface. Cross-well acquisition means that both, sources and receivers, are placed downhole in neighboring boreholes. In this case, $\Delta x_S = \Delta x_G \equiv 0$, assuming vertical boreholes. First aspects of an efficient implementation strategy of the VSP stacking operator (3) are discussed in Boelsen (2005).

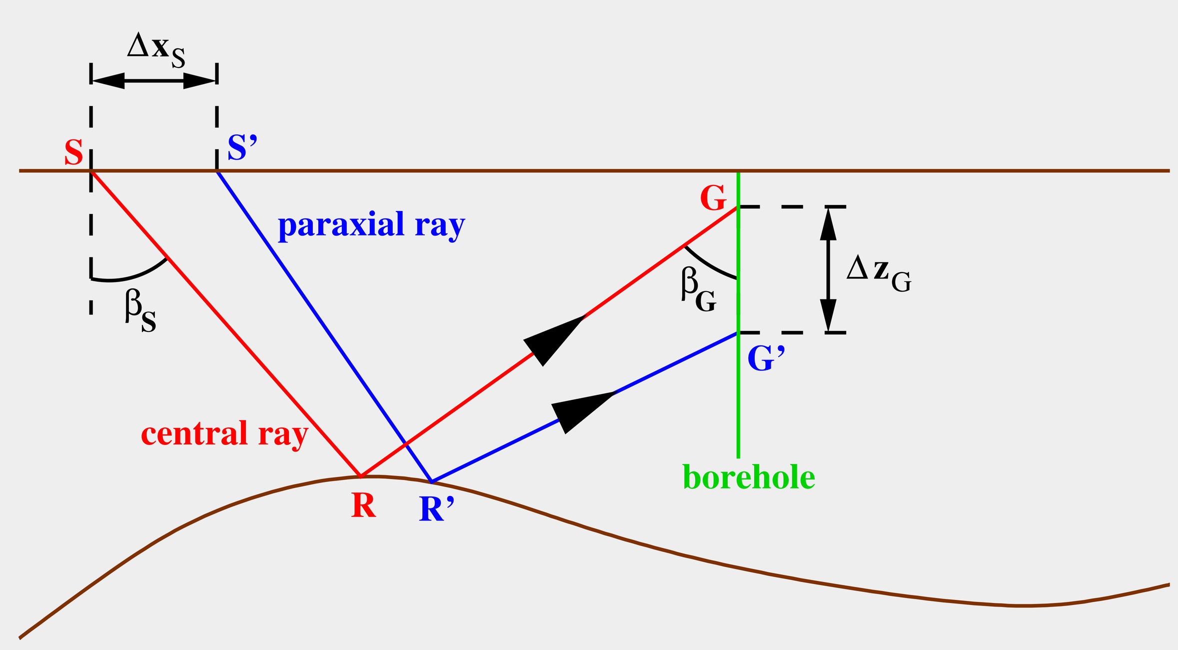

Figure 4: 2D VSP acquisition geometry. An arbitrarily chosen central ray (SRG) and a paraxial ray ($S'R'G'$) in its close vicinity are depicted in red and blue, respectively.

2D CO CRS stack for OBS and VSP data and arbitrary top-surface topography

Tim Boelsen and Jürgen Mann
Geophysical Institute, University of Karlsruhe, Germany

The OBS model setup

In this data example, we apply the 2D CO CRS stack to a complex synthetic OBS data set. The stacking operator is given by Equation (2). Figure 5 shows the blocky P-wave velocity model used to generate the multi-coverage prestack data set. The uppermost layer represents the water layer, the sources are located in a water depth of six meters and the receivers are deployed on the uppermost interface which represents a horizontal ocean bottom at a depth of 1.0 km. For this model, primary PP-reflections were simulated for half-offsets from $h = 0$ km to $h = -2$ km in increments of $\Delta h = 0.025$ km and midpoint intervals of $\Delta m = 0.025$ km in the range $-1.5\,\text{km} \leq m \leq 11.5\,\text{km}$. As seismic signal, a zero-phase Ricker wavelet of 30 Hz peak frequency was used. The sampling interval was 4 ms. Finally, random noise was added to the data set such that all CO prestack sections look with respect to their S/N ratio similar to the one for half-offset $h = -0.5$ km (upper part of Figure 6).

It is the aim of this example to demonstrate the applicability of the CO CRS stack to OBS acquisition geometries. For this purpose, only PP-reflections were modeled. A strategy to handle also converted-wave multi-component data in the framework of the CO CRS stack is presented in Boelsen and Mann (2005).

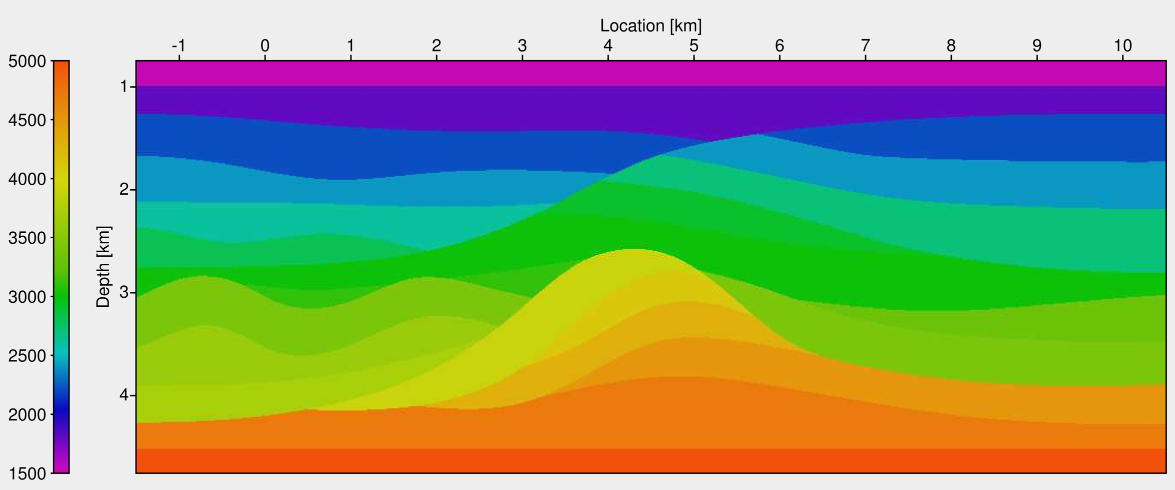

Figure 5: P-wave velocity model [m/s]. The receivers are located on the uppermost interface which represents a horizontal ocean bottom.

2D CO CRS stack results

In the following, we present the final results of the CO CRS stacking procedure. The lower part of Figure 6 shows the CO section for half-offset $h = -0.5$ km simulated with the CO CRS stack. Compared with the respective CO section from the prestack data (upper part of Figure 6) the S/N ratio is dramatically increased and all reflectors are clearly visible. This indicates that the 2D CO CRS stacking operator given by Equation (2) fits well the actual reflection events in the prestack data volume in the vicinity of the respective CO samples. The very high S/N ratio is due to the spatial CRS stacking operator yielding much more traces contributing to the stacking result of each sample of the section to be simulated.

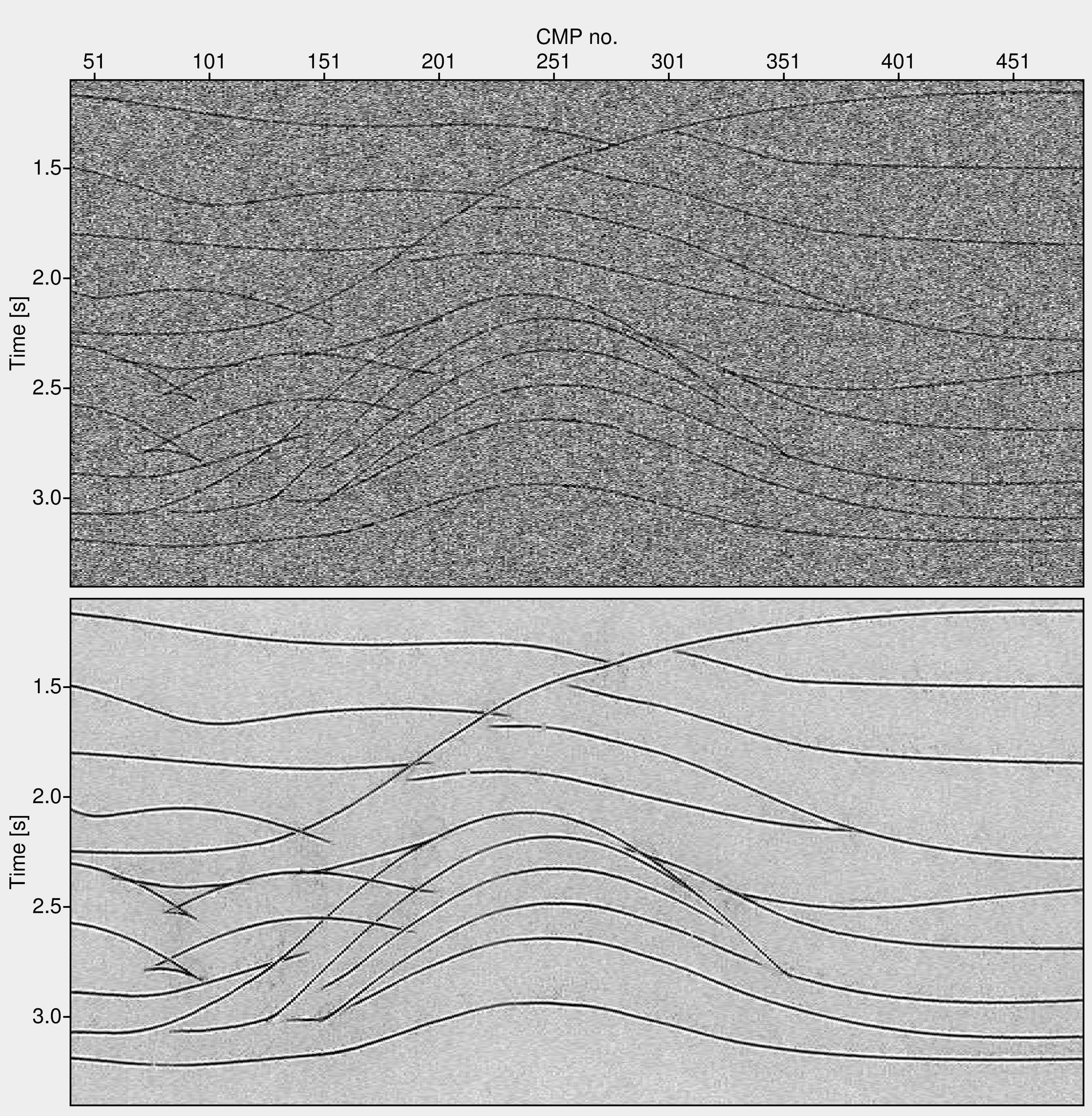

Figure 6: Upper part: CO section ($h = -0.5$ km) taken from the multi-coverage prestack data generated with the model depicted in Figure 5. Lower part: the same CO section simulated with the CO CRS stack.

Kinematic wavefield attributes

The five wavefield attributes β_S, β_G, K_1, K_2, and K_3 can be computed for each sample of the simulated CO section as the near-surface velocities at the receivers and sources are known. Figure 7 shows the incidence and emergence angles as well as the coherence section. Figure 8 depicts the determined wavefront curvatures. For almost all samples along the reflection events, the coherence values are sufficiently high. Thus, the respective wavefield attributes are expected to be reliable.

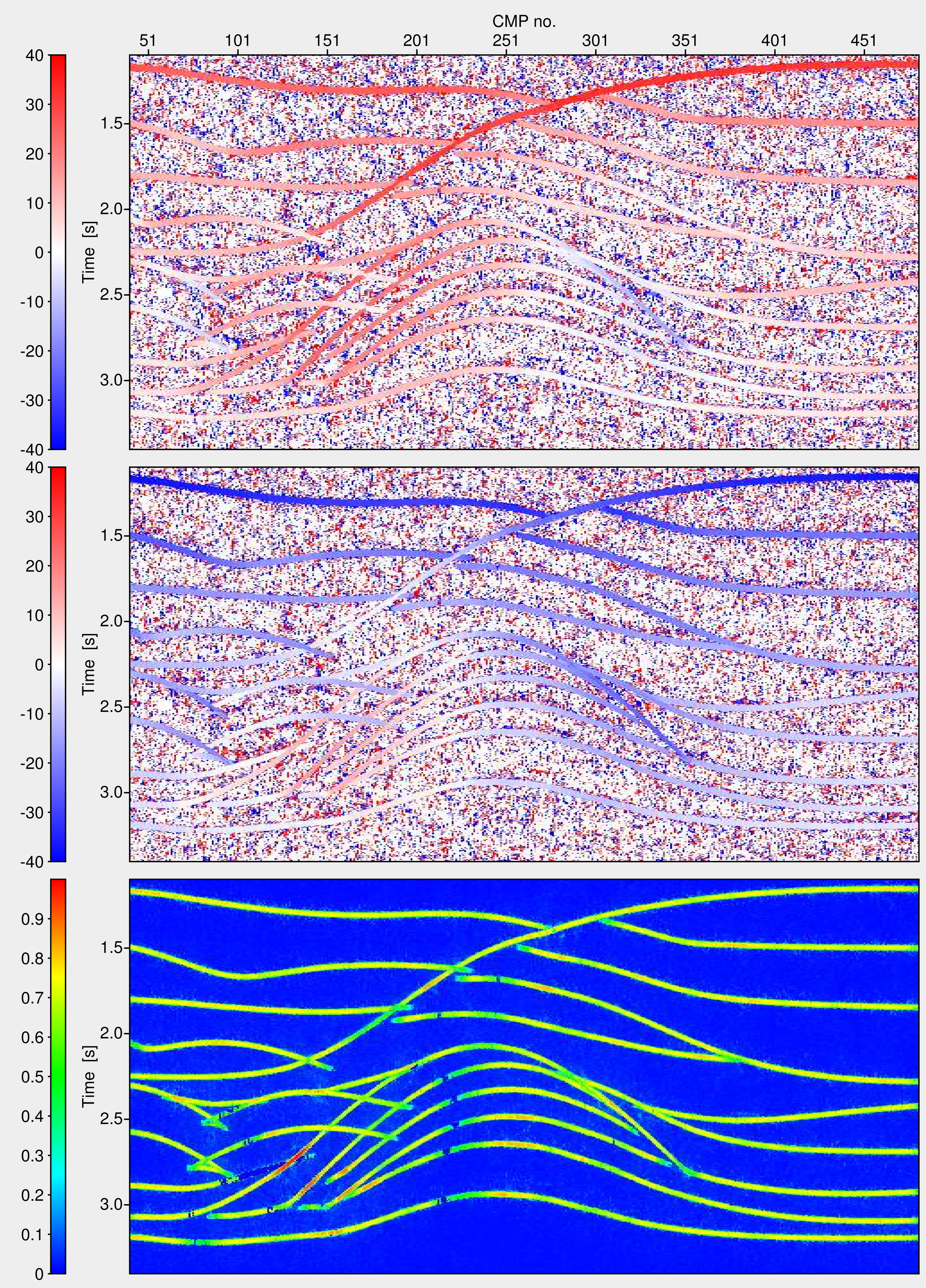

Figure 7: β_S-section [°] (top), β_G-section [°] (middle), and coherence section (bottom) determined by the CO CRS stack.

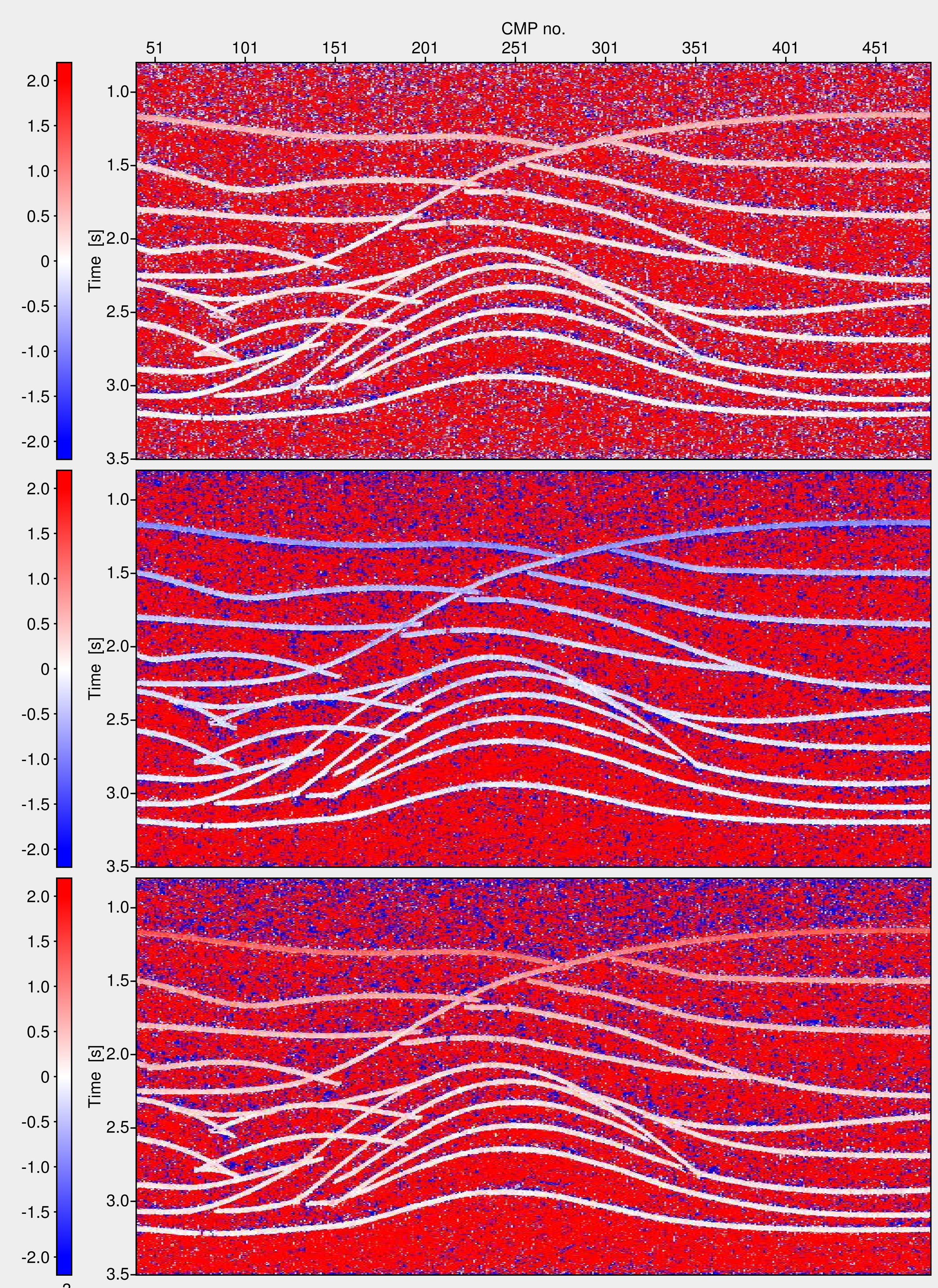

Figure 8: K_1-section (top), K_2-section (middle), and K_3-section (bottom) [1/km] determined by the CO CRS stack.

Conclusions & Outlook

We presented a new hyperbolic paraxial traveltime approximation applicable in the framework of the 2D CO CRS stack to handle arbitrary top-surface topography.

Based on this formula, we derived CRS stacking operators for OBS and VSP acquisition geometries. In case of a virtually horizontal seafloor, the OBS stacking operator turned out to coincide with the original one developed to stack data acquired along one straight line on a horizontal measurement surface. Stacking operators for reverse VSP and cross-well seismics can also be derived.

It is also possible to take varying seafloor elevations (for OBS data) as well as non-vertical boreholes and/or varying surface elevations (for VSP data) into account.

The OBS stacking operator was successfully tested on a complex synthetic data set. We achieved a high-quality stacked section with a high S/N ratio and five kinematic wavefield attribute sections which are useful for further calculations.

The results are of particular interest in combination with multi-component data which can also be handled in the framework of the 2D CO CRS stack in order to obtain stacked sections as well as wavefield attribute sections for PP- and PS-reflections.

Further research will focus on the implementation and test of the VSP stacking operator, also in combination with multi-component data processing. Applications of the CO CRS stack to real data (e. g., OBS data) are also required.

References

Bergler, S. (2001). The Common-Reflection-Surface Stack for Common Offset - Theory and Application. Master's thesis, University of Karlsruhe.

Boelsen, T. (2005). The Common-Reflection-Surface Stack for arbitrary acquisition geometries and multi-component data – Theory and Application. Master's thesis, University of Karlsruhe.

Boelsen, T. and Mann, J. (2005). 2D CO CRS stack for multi-component seismic reflection data. In *Extended abstracts, 67th Conf.* Eur. Assn. Geosci. Eng. Session P063.

Duveneck, E. (2004). Velocity model estimation with data-derived wavefront attributes. *Geophysics*, 69(1):265–274.

Jäger, R., Mann, J., Höcht, G., and Hubral, P. (2001). Common-Reflection-Surface stack: image and attributes. *Geophysics*, 66(1):97–109.

Mann, J., Jäger, R., Müller, T., Höcht, G., and Hubral, P. (1999). Common-Reflection-Surface stack – a real data example. *J. Appl. Geophys.*, 42(3,4):301–318.

Müller, N.-A. (2005). 3-D inversion with kinematic wavefield attributes. In *Extended abstracts, 67th Conf.* Eur. Assn. Geosci. Eng. Session B040.

Zhang, Y. (2003). *Common-Reflection-Surface Stack and the Handling of Top Surface Topography*. Logos Verlag, Berlin.

Zhang, Y., Bergler, S., and Hubral, P. (2001). Common-Reflection-Surface (CRS) stack for common-offset. *Geophys. Prosp.*, 49(6):709–718.

Acknowledgments

This work was kindly supported by the sponsors of the *Wave Inversion Technology (WIT) Consortium*, Karlsruhe, Germany.

Related presentations

B040 3-D inversion with kinematic wavefield attributes, *N.-A. Müller*

F042 Minimum-aperture Kirchhoff migration by means of CRS attributes, *C. Jäger*

P012 CRS-stack-based seismic imaging considering top-surface topography, *von Steht et al.*

P063 2D CO CRS stack for multi-component seismic reflection data, *Boelsen and Mann*

W6-03 CRS-stack-based seismic imaging considering top-surface topography, *Z. Heilmann*

W6-04 CRS-stack-based residual static correction – a real data example, *I. Koglin*

W6-05 The application of CRS methods to a line from Saudi Arabia, *G. Gierse*